

Spectrum and electromagnetic transitions of bottomonium

Wei-Jun Deng, Hui Liu, Long-Cheng Gui* and Xian-Hui Zhong†

1) Department of Physics, Hunan Normal University, Changsha 410081, China

2) Synergetic Innovation Center for Quantum Effects and Applications (SICQEA), Changsha 410081, China and

3) Key Laboratory of Low-Dimensional Quantum Structures and Quantum Control of Ministry of Education, Changsha 410081, China

Stimulated by the recently exciting progress in the observation of new bottomonium states, we study the bottomonium spectrum. To calculate the mass spectrum, we adopted a nonrelativistic screened potential model. The radial Schrödinger equation is solved with the three-point difference central method, where the spin-dependent potentials are dealt with non-perturbatively. With this treatment, the corrections of the spin-dependent potentials to the wavefunctions can be included successfully. Furthermore, we have calculated the electromagnetic transitions of the nS , nP ($n \leq 3$), and nD ($n \leq 2$) bottomonium states with a nonrelativistic electromagnetic transition operator widely applied to meson photoproduction reactions. Our calculated masses, hyperfine and fine splittings, and electromagnetic transition rates for the bottomonium states are in good agreement with the available experimental data. We hope our study can provide some useful references to determine the properties of the bottomonium states in forthcoming experiments.

PACS numbers: 14.40.Pq, 13.20.Gd, 12.39.Jh

I. INTRODUCTION

Bottomonium is considered to be an excellent laboratory to study Quantum Chromodynamics (QCD) at low energies [1, 2]. Due to a relatively large mass of the heavy bottom quark, the bottomonium system is essentially nonrelativistic, which makes it relatively easy for people to study the perturbative and nonperturbative QCD via the bottomonium spectroscopy with a nonrelativistic approximation. In the past few years, great progress has been achieved in the study of the bottomonium spectroscopy [3–6]. A fairly abundant bottomonium states have been established in experiments [7] (see Tab. I). Furthermore, many new experiments are being and/or to be carried out at LHC and Belle. In near future, more missing bottomonium states will be discovered and more decay channels will be measured in experiments. Thus, it is necessary to systematically carry out a study of the bottomonium states according to the recent progress. On the one hand we can obtain more knowledge of bottomonium states from experiments. On the other hand, the predicted properties can provide some useful references for our search for the missing bottomonium states in experiments.

In recent years, stimulated by the exciting progress in experiments, many theoretical studies of bottomonium spectrum have been carried out with different methods, such as the widely used potential models [8–14], lattice QCD [15–18], effective Lagrangian approach [19], nonrelativistic effective field theories of QCD [20–22], various coupled-channel quark models [23, 24], and light front quark model [25–28]. Although some comparable predictions from different models, strong model dependencies still exist in the predictions. For example, the recent calculations with the relativized quark model [9] give a successful prediction of masses for the low-lying excitations, however, its predicted mass for the higher

excitation $\Upsilon(6S)$ is about 80 MeV higher than the data. While the recent nonrelativistic constituent quark model [10] gives a good description of the mass for $\Upsilon(6S)$, however, its predictions of the masses for the ground states $\Upsilon(1S)$ and $\eta_b(1S)$ are about 50 MeV larger than the experimental values. Furthermore, about the M1 transitions of $\Upsilon(2S, 3S) \rightarrow \eta_b(1S)\gamma$, the predictions from the relativistic quark model [13] and nonrelativistic effective field theories of QCD [22] are about an order of magnitude smaller than the recent predictions from the relativized quark model [9] and nonrelativistic constituent quark model [10]. Thus, to deepen our knowledge about the bottomonium spectrum, more theoretical studies are needed.

In this work, firstly we use the non-relativistic screened potential model [8, 29–31] to calculate the masses and wavefunctions. In this model, the often used linear potential br is replaced with the screened potential $b(1 - e^{-\mu r})/\mu$. The reason is that the linear potential, which is expected to be dominant at large distances, is screened or softened by the vacuum polarization effect of the dynamical light quark pairs [32, 33]. Such a screening effect might be important for us to reasonably describe the higher radial and orbital excitations. In Ref. [8], the spin-dependent interactions were considered perturbatively when they calculated the bottomonium spectrum. Considering the corrections of the spin-dependent interactions to the space wavefunctions can not be included with the perturbative treatment, we treat the spin-dependent interactions as non-perturbations in our calculations. With the nonperturbative treatment, we can reasonably include the effect of spin-dependent interactions on the wavefunctions, which is important for us to gain reliable predictions of the decays.

Moreover, using the wavefunctions, we study the electromagnetic (EM) transitions between bottomonium states. Difference of our method from the often used potential models is that the EM transition operator between initial and final hadron states is used a special nonrelativistic form $h_e \simeq \sum_j [e_j \mathbf{r}_j \cdot \boldsymbol{\epsilon} - \frac{e_j}{2m_j} \boldsymbol{\sigma}_j \cdot (\boldsymbol{\epsilon} \times \hat{\mathbf{k}})] e^{-i\mathbf{k} \cdot \mathbf{r}_j}$ [34], which has been well developed and widely applied to meson photoproduction reactions [35–45]. In this operator, the effects of binding potential between quarks is considered. Furthermore, the possible

*E-mail: guilongcheng@ihcp.ac.cn

†E-mail: zhongxh@hunnu.edu.cn

higher EM multipole contributions to a EM transition process can be included naturally.

The paper is organized as follows. In Sec. II, we calculate the masses and wavefunctions within a screened potential model. In Sec. III, the EM transitions between states are calculated, and our analysis and discussion are given. Finally, a summary is given in Sec. IV.

TABLE I: Bottomonium spectrum calculated by us. For comparison, the measured masses (MeV) from the PDG [7], and the theoretical predictions with the previous screened potential model [8], relativized quark model [9], and nonrelativistic constituent quark model [10] are also listed in the same table.

$n^{2S+1}L_J$	name	J^{PC}	Exp. [7]	[8]	[9]	[10]	Ours
1^3S_1	$\Upsilon(1S)$	1^{--}	9460	9460	9465	9502	9460
1^1S_0	$\eta_b(1S)$	0^{++}	9398	9389	9402	9455	9390
2^3S_1	$\Upsilon(2S)$	1^{--}	10023	10016	10003	10015	10015
2^1S_0	$\eta_b(2S)$	0^{++}	9999	9987	9976	9990	9990
3^3S_1	$\Upsilon(3S)$	1^{--}	10355	10351	10354	10349	10343
3^1S_0	$\eta_b(3S)$	0^{++}		10330	10336	10330	10326
4^3S_1	$\Upsilon(4S)$	1^{--}	10579	10611	10635	10607	10597
4^1S_0	$\eta_b(4S)$	0^{++}		10595	10623		10584
5^3S_1	$\Upsilon(5S)$	1^{--}	10865	10831	10878	10818	10811
5^1S_0	$\eta_b(5S)$	0^{++}		10817	10869		10800
6^3S_1	$\Upsilon(6S)$	1^{--}	11020	11023	11102	10995	10997
6^1S_0	$\eta_b(6S)$	0^{++}		11011	11097		10988
1^3P_2	$\chi_{b2}(1P)$	2^{++}	9912	9918	9897	9886	9921
1^3P_1	$\chi_{b1}(1P)$	1^{++}	9893	9897	9876	9874	9903
1^3P_0	$\chi_{b0}(1P)$	0^{++}	9859	9865	9847	9855	9864
1^1P_1	$h_b(1P)$	1^{+-}	9899	9903	9882	9879	9909
2^3P_2	$\chi_{b2}(2P)$	2^{++}	10269	10269	10261	10246	10264
2^3P_1	$\chi_{b1}(2P)$	1^{++}	10255	10251	10246	10236	10249
2^3P_0	$\chi_{b0}(2P)$	0^{++}	10233	10226	10226	10221	10220
2^1P_1	$h_b(2P)$	1^{+-}	10260	10256	10250	10240	10254
3^3P_2	$\chi_{b2}(3P)$	2^{++}		10540	10550	10521	10528
3^3P_1	$\chi_{b1}(3P)$	1^{++}	10516	10524	10538	10513	10515
3^3P_0	$\chi_{b0}(3P)$	0^{++}		10502	10522	10500	10490
3^1P_1	$h_b(3P)$	1^{+-}		10529	10541	10516	10519
1^3D_3	$\Upsilon_3(1D)$	3^{--}		10156	10155	10127	10157
1^3D_2	$\Upsilon_2(1D)$	2^{--}	10164	10151	10147	10122	10153
1^3D_1	$\Upsilon_1(1D)$	1^{--}		10145	10138	10117	10146
1^1D_2	$\eta_{b2}(1D)$	2^{++}		10152	10148	10123	10153
2^3D_3	$\Upsilon_3(2D)$	3^{--}		10442	10455	10422	10436
2^3D_2	$\Upsilon_2(2D)$	2^{--}		10438	10449	10418	10432
2^3D_1	$\Upsilon_1(2D)$	1^{--}		10432	10441	10414	10425
2^1D_2	$\eta_{b2}(2D)$	2^{++}		10439	10450	10419	10432
1^1F_3	$h_{b3}(1F)$	3^{+-}			10355	10322	10339
1^3F_4	$\chi_{b4}(1F)$	4^{++}			10358		10340
1^3F_3	$\chi_{b3}(1F)$	3^{++}			10355	10321	10340
1^3F_2	$\chi_{b2}(1F)$	2^{++}			10350	10315	10338

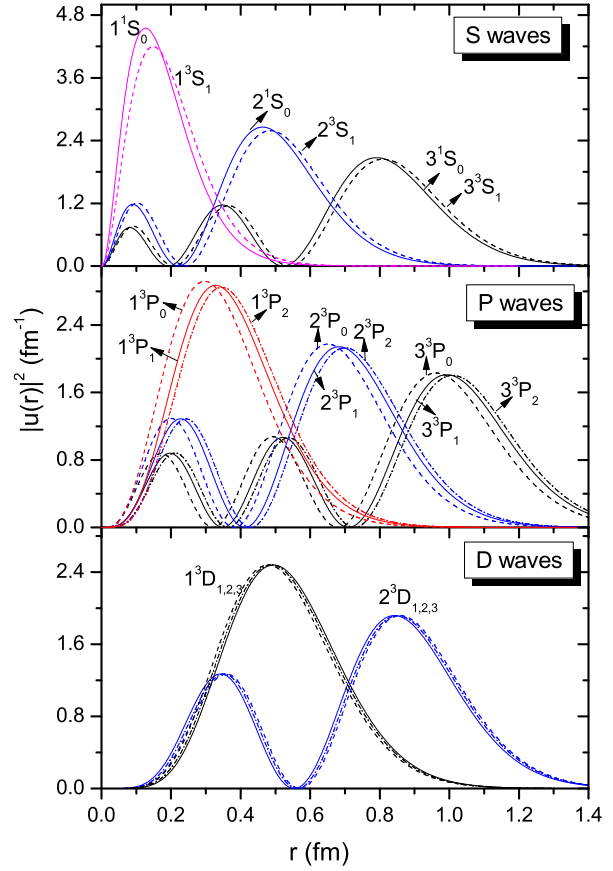


FIG. 1: (Color online) Predicted radial probability density $|u(r)|^2$ for S -, P - and D -wave bottomonium states.

II. MASS SPECTRUM

As a minimal model of the bottomonium system we use a nonrelativistic screened potential model [8, 29–31]. The effective potential of spin-independent term $V(r)$ is regarded as the sum of Lorentz vector $V_V(r)$ and Lorentz scalar $V_s(r)$ contributions [3], i.e.,

$$V(r) = V_V(r) + V_s(r). \quad (1)$$

The Lorentz vector potential $V_V(r)$ is adopted the standard color Coulomb form:

$$V_V(r) = -\frac{4}{3} \frac{\alpha_s}{r}. \quad (2)$$

To take into account the screening effects, which might originate from the vacuum polarization of the dynamical light quark pairs [32, 33], the widely used linear scalar potential br is replaced with a special form

$$V_s(r) = \frac{b(1 - e^{-\mu r})}{\mu}, \quad (3)$$

TABLE II: Hyperfine and fine splittings in units of MeV for bottomonium in our calculation. The experimental data are taken from the PDG [7]. The theoretical predictions with the previous screened potential model [8], relativized quark model [9], relativistic two-body calculation [11], and nonrelativistic constituent quark model [10, 12] are also listed in the same table for comparison.

Δm	Ours	[8]	[9]	[10]	[11]	[12]	Exp. [7]
$m(1^3S_1)-m(1^1S_0)$	70	71	63	47	76	49	62.3 ± 3.2
$m(2^3S_1)-m(2^1S_0)$	25	29	27	25	38	16	$24.3^{+4.0}_{-4.5}$
$m(3^3S_1)-m(3^1S_0)$	17	21	18	19		11	
$m(4^3S_1)-m(4^1S_0)$	13	16	12			11	
$m(5^3S_1)-m(5^1S_0)$	11	14	9			15	
$m(6^3S_1)-m(6^1S_0)$	9	12	5				
$m(1^3P_2)-m(1^3P_1)$	18	21	21	12	22	18	19.43 ± 0.57
$m(1^3P_1)-m(1^3P_0)$	39	32	29	19	29	48	33.34 ± 0.66
$m(2^3P_2)-m(2^3P_1)$	15	18	15	10	18	16	13.19 ± 0.77
$m(2^3P_1)-m(2^3P_0)$	29	25	20	15	24	40	22.96 ± 0.84
$m(3^3P_2)-m(3^3P_1)$	13	16	12	8		14	
$m(3^3P_1)-m(3^3P_0)$	25	22	16	13		36	

as suggested in Refs. [8, 29–31]. Here μ is the screening factor which makes the long-range scalar potential of $V_s(r)$ behave like br when $r \ll 1/\mu$, and becomes a constant b/μ when $r \gg 1/\mu$. The main effect of the screened potential on the spectrum is that the masses of the higher excited states are lowered. Such a screening effect might be important for us to reasonably describe the higher radial and orbital excitations.

We include three spin-dependent potentials as follows. For the spin-spin contact hyperfine potential, we take [46]

$$H_{SS} = \frac{32\pi\alpha_s}{9m_b^2} \tilde{\delta}_\sigma(r) \mathbf{S}_b \cdot \mathbf{S}_{\bar{b}}, \quad (4)$$

where \mathbf{S}_b and $\mathbf{S}_{\bar{b}}$ are spin matrices acting on the spins of the quark and antiquark. We take $\tilde{\delta}_\sigma(r) = (\sigma/\sqrt{\pi})^3 e^{-\sigma^2 r^2}$ as in Ref. [46]. The five parameters in the above equations (α_s , b , μ , m_b , σ) are determined by fitting the spectrum.

For the spin-orbit term and the tensor term, we take the common forms [3]:

$$H_{SL} = \frac{1}{2m_b^2 r} \left(3 \frac{dV_V}{dr} - \frac{dV_s}{dr} \right) \mathbf{L} \cdot \mathbf{S}, \quad (5)$$

and

$$H_T = \frac{1}{12m_b^2} \left(\frac{1}{r} \frac{dV_V}{dr} - \frac{d^2 V_V}{dr^2} \right) S_T, \quad (6)$$

where \mathbf{L} is the relative orbital angular momentum of b and \bar{b} quarks, $\mathbf{S} = \mathbf{S}_b + \mathbf{S}_{\bar{b}}$ is the total quark spin, and the spin tensor S_T is defined by [3]

$$S_T = 6 \frac{\mathbf{S} \cdot \mathbf{rS} \cdot \mathbf{r}}{r^2} - 2\mathbf{S}^2. \quad (7)$$

In the $|^{2S+1}L_J\rangle$ basis, the matrix element for the spin-spin operator $\mathbf{S}_b \cdot \mathbf{S}_{\bar{b}}$ is

$$\langle \mathbf{S}_b \cdot \mathbf{S}_{\bar{b}} \rangle = \frac{1}{2} S(S+1) - \frac{3}{4}. \quad (8)$$

For the spin-orbit operator $\mathbf{L} \cdot \mathbf{S}$, its matrix element is

$$\langle \mathbf{L} \cdot \mathbf{S} \rangle = \frac{1}{2} [J(J+1) - L(L+1) - S(S+1)]. \quad (9)$$

The element of tensor operator S_T can be written in the form [47]

$$\langle S_T \rangle = \frac{4\langle \mathbf{S}^2 \mathbf{L}^2 - \frac{3}{2} \mathbf{L} \cdot \mathbf{S} - 3(\mathbf{L} \cdot \mathbf{S})^2 \rangle}{(2L+3)(2L-1)}. \quad (10)$$

To obtain masses and wavefunctions of the bottomonium states, we need solve the radial Schrödinger equation

$$\frac{d^2 u(r)}{dr^2} + 2\mu_R \left[E - V_{b\bar{b}}(r) - \frac{L(L+1)}{2\mu_R r^2} \right] u(r) = 0, \quad (11)$$

with

$$V_{b\bar{b}}(r) = V(r) + H_{SS} + H_{SL} + H_T, \quad (12)$$

where $\mu_R = m_b m_{\bar{b}} / (m_b + m_{\bar{b}})$ is the reduced mass of the system. In Ref. [8], the spin-dependent interactions were dealt with perturbatively. Although the meson mass obtains perturbative corrections from these spin-dependent potentials, the wave functions obtain no corrections from these spin-dependent potentials. To reasonably include the corrections from these spin-dependent potentials to both the mass and wave function of a meson state, we deal with the spin-dependent interactions non-perturbatively.

In this work, we solve the radial Schrödinger equation by using the three-point difference central method from central ($r=0$) towards outside ($r \rightarrow \infty$) point by point. The details of this method can be found in Ref. [48]. In this method, we need know the role of $u(r \rightarrow 0)$. Without the contributions of the spin-orbit and tensor terms, we easily obtain $u(r \rightarrow 0) \propto r^{L+1}$. However, including the spin-orbit and tensor potential contributions, we have a term $\propto 1/r^3$ in the potential. In the limit $r \rightarrow 0$, the potential $V_{b\bar{b}}(r) \propto 1/r^3$. In this case, we do not know the role of $u(r \rightarrow 0)$, thus, we can not solve the radial Schrödinger equation with the three-point differential central method. To overcome this problem, we assume that in a small range $r \in (0, r_c)$, the $V_{b\bar{b}}(r) \propto 1/r_c^3$, which is a finite constant. Then, the role of $u(r \rightarrow 0)$ is still $\propto r^{L+1}$. The price of our method is that a cutoff distance r_c should be introduced in the calculation, which is determined by fitting the spectrum.

For the model parameters, we take $\alpha_s = 0.368$, $b = 0.206$ GeV², $\mu = 0.056$ GeV, $m_b = 4.757$ GeV, and $\sigma = 3.10$ GeV. This parameter set is slightly different from that suggested in Ref. [8]. In our calculation, the cutoff distance $r_c = 0.06$ fm is adopted.

With these parameters, by solving the radial Schrödinger equation we obtain the mass spectrum, which have been listed in Tab I. From the table, we can see that our results are compatible with the previous screened potential model predictions [8], which indicates that our numerical method is reliable. The recent relativized quark model can successfully describe the low-lying bottomonium states, however, their predicted masses for the higher excitations $\Upsilon(4S)$ and $\Upsilon(6S)$ are about 60 ~ 80 MeV larger than the experimental measurements [9]. Although the recent nonrelativistic constituent

quark model systematically improve the descriptions of the higher mass spectrum, their predicted masses for the ground states $\Upsilon(1S)$ and $\eta_b(1S)$ are about 40 ~ 50 MeV higher than the data [10]. Interestingly, it is found that the screened potential model obtains a fairly good description of the masses not only for the low-lying states, but also for the higher excitations.

Furthermore, in Tab. II, we give our predictions of the hyperfine splittings for some S -wave states, and fine splittings for some P -wave states. For comparison, the world average data from the PDG [7] and some other model predictions in Refs. [8–12] are listed in the same table as well. It is found that our predicted splittings are in good agreement with the world average data [7]. Comparing the predictions from different models with each other, we can find obvious model dependencies in them. Thus, to better understand these nonperturbative QCD, more model-independent studies are needed.

In order to clearly see the properties of the wavefunctions, we plot the radial probability density of the states as a function of the interquark distance r in Fig. 1. It is found that the spin-dependent potentials have notable corrections to the S and triplet P wave states, however, the corrections to the triplet D wave states are tiny. The strong attractive spin-spin potential H_{SS} shifts the wavefunctions of the 1S_0 states towards the center, while the strong attractive tensor potential H_T shifts the wavefunctions of the $^3P_{0,1}$ states towards the center.

III. ELECTROMAGNETIC TRANSITIONS

With these obtained wavefunctions of the bottomonium states, we further study their EM transitions. The quark-photon EM coupling at the tree level is adopted as

$$H_e = - \sum_j e_j \bar{\psi}_j \gamma_\mu^j A^\mu(\mathbf{k}, \mathbf{r}) \psi_j, \quad (13)$$

where ψ_j stands for the j -th quark field in a hadron. The photon has three momentum \mathbf{k} , and the constituent quark ψ_j carries a charge e_j .

To match the nonrelativistic wave functions of the bottomonium states, we should adopt the nonrelativistic form of Eq. (13) in the calculations. For the EM transition of a hadron, in the initial-hadron-rest system the nonrelativistic expansion of H_e in Eq.(13) becomes [34, 36]

$$h_e \simeq \sum_j \left[e_j \mathbf{r}_j \cdot \boldsymbol{\epsilon} - \frac{e_j}{2m_j} \boldsymbol{\sigma}_j \cdot (\boldsymbol{\epsilon} \times \hat{\mathbf{k}}) \right] \phi. \quad (14)$$

For emitting a photon, we have $\phi = e^{-i\mathbf{k}\cdot\mathbf{r}_j}$, while for absorbing a photon we have $\phi = e^{+i\mathbf{k}\cdot\mathbf{r}_j}$. It is found that the first and second terms in Eq.(14) are responsible for the electric and magnetic transitions respectively. The main feature of this EM transition operator is that the effects of binding potential between quarks is considered. Furthermore, the possible higher EM multipole contributions are included naturally. This nonrelativistic form has been widely applied to meson photoproduction reactions [35–45].

Then, one obtains the standard helicity amplitude \mathcal{A} of the radiative decay process by the relation

$$\mathcal{A} = -i \sqrt{\frac{\omega_\gamma}{2}} \langle f | h_e | i \rangle. \quad (15)$$

Finally, we can calculate the EM decay width by

$$\Gamma = \frac{|\mathbf{k}|^2}{\pi} \frac{2}{2J_i + 1} \frac{M_f}{M_i} \sum_{J_{fz}, J_{iz}} |\mathcal{A}_{J_{fz}, J_{iz}}|^2, \quad (16)$$

where J_i is the total angular momenta of the initial mesons, J_{fz} and J_{iz} are the component of the total angular momentum along the z axis of initial and final mesons, respectively. In the calculation, for the well-established bottomonium states, their masses are adopted the experimental average values from the PDG [7]. While for the missing bottomonium states, their masses are adopted from our theoretical predictions.

A. $\Upsilon(1S) \rightarrow \eta_b(1S)\gamma$

The $\Upsilon(1S) \rightarrow \eta_b(1S)\gamma$ decay process is a typical M1 transition at tree level, which is strongly suppressed by the constituent bottom quark mass m_b . Our predicted partial width is

$$\Gamma[\Upsilon(1S) \rightarrow \eta_b(1S)\gamma] \simeq 10 \text{ eV}. \quad (17)$$

Combined with the width of $\Upsilon(1S)$, our predicted branching ratio

$$\mathcal{B}[\Upsilon(1S) \rightarrow \eta_b(1S)\gamma] \simeq 2.0 \times 10^{-4}. \quad (18)$$

Our predictions are in good agreement with the recent predictions from the relativized quark model [9] and nonrelativistic constituent quark model [10] (see tab. III). However, our prediction of the $\Gamma[\Upsilon(1S) \rightarrow \eta_b(1S)\gamma]$ is larger than the value 5.8 eV from the relativistic quark model [13], while smaller than the recent prediction 15.2 eV from the pNRQCD approach [22]. It should be mentioned that this decay rate is extremely sensitive to the masses of $\Upsilon(1S)$ and $\eta_b(1S)$. If all of the models adopt the experimental masses, the prediction of $\Gamma[\Upsilon(1S) \rightarrow \eta_b(1S)\gamma]$ from different model might be consistent with each other.

B. Radiative transitions of $2S$ states

1. $\Upsilon(2S)$

The allowed EM transitions of $\Upsilon(2S)$ are $\Upsilon(2S) \rightarrow \chi_{bJ}(1P)\gamma$ and $\Upsilon(2S) \rightarrow \eta_b(1S, 2S)\gamma$. The $\Upsilon(2S) \rightarrow \chi_{bJ}(1P)\gamma$ processes are governed by the E1 transitions. While $\Upsilon(2S) \rightarrow \eta_b(1S, 2S)\gamma$ are typical M1 transitions.

Our predicted partial decay widths for the $\psi(2S) \rightarrow \chi_{cJ}(1P)\gamma$ processes are

$$\Gamma[\Upsilon(2S) \rightarrow \chi_{b0}(1P)\gamma] \simeq 1.09 \text{ keV}, \quad (19)$$

$$\Gamma[\Upsilon(2S) \rightarrow \chi_{b1}(1P)\gamma] \simeq 2.17 \text{ keV}, \quad (20)$$

$$\Gamma[\Upsilon(2S) \rightarrow \chi_{b2}(1P)\gamma] \simeq 2.62 \text{ keV}, \quad (21)$$

TABLE III: Partial widths of the M1 radiative transitions for some low-lying S - and P -wave bottomonium states. For comparison, the measured values (MeV) from the PDG [7], and the theoretical predictions with the relativistic quark model [13], nonrelativistic effective field theories of QCD [22], relativized quark model [9], and nonrelativistic constituent quark model [10] are also listed in the same table.

Initial meson state	Final meson state	E_γ (MeV)			Γ_{M1} (eV)					Γ_{M1} (eV) Exp. [7]
		Ref.[13]	Ref. [9]	ours	Ref.[13]	Ref. [9]	Ref. [22]	Ref. [10]	Ours	
$\Upsilon(1^3S_1)$	$\eta_b(1^1S_0)$	60	62	62	5.8	10	15.2	9.34	10	
$\Upsilon(2^3S_1)$	$\eta_b(2^1S_0)$	33	24	24	1.4	0.59	0.67	0.58	0.59	
$\eta_b(2^1S_0)$	$\eta_b(1^1S_0)$	604	606	606	6.4	81	6_{-6}^{+26}	56.5	66	12.5 ± 4.9
	$\Upsilon(1^3S_1)$	516	524	524	12	68	~ 80	45.0	64	
$\Upsilon(3^3S_1)$	$\eta_b(3^1S_0)$	27	18	18	0.8	0.25		0.66	3.9	< 14 10 ± 2
	$\eta_b(2^1S_0)$	359	350	350	1.5	0.19		11.0	11	
	$\eta_b(1^1S_0)$	911	913	913	11	60		57.0	71	
$\eta_b(3^1S_0)$	$\Upsilon(2^3S_1)$	301	309	309	2.8	9.1		9.20	8.7	
	$\Upsilon(1^3S_1)$	831	840	840	24	74		51.0	60	
$\chi_{b2}(1^3P_2)$	$h_b(1^1P_1)$		13	13		9.6×10^{-2}	0.12	8.9×10^{-2}	9.5×10^{-2}	
$h_b(1^1P_1)$	$\chi_{b1}(1^3P_1)$		6	6		1.0×10^{-2}	9.0×10^{-3}	1.15×10^{-2}	9.4×10^{-3}	
	$\chi_{b0}(1^3P_0)$		40	40		0.89	0.96	0.86	0.90	
$\chi_{b2}(2^3P_2)$	$h_b(1^1P_1)$		363	363		0.24		1.78	4.5	
$\chi_{b1}(2^3P_1)$			350	350		2.2		0.17	0.18	
$\chi_{b0}(2^3P_0)$			329	329		9.7		2.39	16	
$h_b(2^1P_1)$	$\chi_{b2}(1^3P_2)$		342	342		2.2		6.91×10^{-3}	1.1	
	$\chi_{b1}(1^3P_1)$		360	360		1.1		1.28	2.5	
	$\chi_{b0}(1^3P_0)$		393	393		0.32		36.4	10	

which are in good agreement with the world average data from the PDG [7], and also are consistent with predictions from various potential models [8–13].

For the M1 transitions $\Upsilon(2S) \rightarrow \eta_b(1S)\gamma$ and $\eta_b(2S)\gamma$, our predicted partial decay widths are

$$\Gamma[\Upsilon(2S) \rightarrow \eta_b(1S)\gamma] \simeq 6.6 \times 10^{-2} \text{ keV}, \quad (22)$$

$$\Gamma[\Upsilon(2S) \rightarrow \eta_b(2S)\gamma] \simeq 5.9 \times 10^{-4} \text{ keV}. \quad (23)$$

Our result for $\Gamma[\Upsilon(2S) \rightarrow \eta_b(1S)\gamma]$ is compatible with the recent potential model predictions [9, 10], however, it is 5 times larger than the average value $1.25(49) \times 10^{-2}$ keV from the PDG [7] and the recent lattice NRQCD result $1.72(55) \times 10^{-2}$ keV [15]. More studies of the M1 transition of $\Upsilon(2S) \rightarrow \eta_b(1S)\gamma$ are needed in both theory and experiments.

2. $\eta_b(2S)$

The $\eta_b(2S)$ resonance can decay into $h_b(1P)\gamma$ and $\Upsilon(1S)\gamma$ channels by the E1 and M1 transitions, respectively. Our predicted partial decay width

$$\Gamma[\eta_b(2S) \rightarrow h_b(1P)\gamma] \simeq 3.41 \text{ keV}, \quad (24)$$

is in good agreement with the predictions of the relativistic quark model [13], potential model [9], and nonrelativistic constituent quark model [10] (see Tab. IV). Our result is about a factor 1.8 smaller than the previous SNR model prediction [8]. This difference might come from the corrections of the spin-dependent potentials to the wavefunction of $\eta_b(2S)$.

Furthermore, our predicted partial decay width for the M1 transition

$$\Gamma[\eta_b(2S) \rightarrow \Upsilon(1S)\gamma] \simeq 64 \text{ eV}, \quad (25)$$

is compatible with the recent predictions of potential models [9, 10], and pNRQCD approach [22]. However, our prediction is notably larger than the value of $\Gamma[\eta_b(2S) \rightarrow \Upsilon(1S)\gamma] \simeq 12 \text{ eV}$ predicted with a relativistic quark model [13] (see Tab. III).

C. Radiative transitions of $1P$ states

1. $\chi_{bJ}(1P)$

The typical radiative transitions of $\chi_{bJ}(1P)$ are $\chi_{bJ}(1P) \rightarrow \Upsilon(1S)\gamma$. Our results

$$\Gamma[\chi_{b0}(1P) \rightarrow \Upsilon(1S)\gamma] \simeq 27.5 \text{ keV}, \quad (26)$$

$$\Gamma[\chi_{b1}(1P) \rightarrow \Upsilon(1S)\gamma] \simeq 31.9 \text{ keV}, \quad (27)$$

$$\Gamma[\chi_{b2}(1P) \rightarrow \Upsilon(1S)\gamma] \simeq 31.8 \text{ keV}, \quad (28)$$

are in agreement with the predictions in [8–10, 12, 13]. Combining them with the measured branching ratios $\mathcal{B}[\chi_{b0}(1P) \rightarrow \Upsilon(1S)\gamma] \simeq 1.76\%$, $\mathcal{B}[\chi_{b1}(1P) \rightarrow \Upsilon(1S)\gamma] \simeq 33.9\%$, and $\mathcal{B}[\chi_{b2}(1P) \rightarrow \Upsilon(1S)\gamma] \simeq 19.1\%$ [7], we easily estimate the total widths for $\chi_{b0}(1P)$, $\chi_{b1}(1P)$ and $\chi_{b2}(1P)$. They are

$$\Gamma_{\chi_{b0}(1P)}^{\text{total}} \simeq 1.56 \text{ MeV}, \quad (29)$$

$$\Gamma_{\chi_{b1}(1P)}^{\text{total}} \simeq 0.09 \text{ MeV}, \quad (30)$$

$$\Gamma_{\chi_{b2}(1P)}^{\text{total}} \simeq 0.17 \text{ MeV}, \quad (31)$$

respectively. Interestingly, we find that the estimated width for $\chi_{b0}(1P)$ is consistent with the recent measurement 1.3 ± 0.9 MeV from the Belle Collaboration [49].

2. $h_b(1P)$

For the singlet $1P$ state $h_b(1P)$, its main radiative transition is $h_b(1P) \rightarrow \eta_b(1P)\gamma$. We predict that

$$\Gamma[h_b(1P) \rightarrow \eta_b(1P)\gamma] = 35.8 \text{ keV}, \quad (32)$$

which is consistent with various potential model predictions [8, 9, 13] (see Tab. V). Combining the measured branching ratio $\mathcal{B}[h_b(1P) \rightarrow \eta_b\gamma] \simeq 49\%$ [7] and our predicted partial width, we estimate that the total width of $h_b(1P)$ might be $\Gamma_{h_b(1P)}^{\text{total}} \simeq 73$ keV, which could be tested in future experiments.

Finally, we give our estimations of the typical M1 transitions $h_b(1P) \rightarrow \chi_{b0}(1P)\gamma, \chi_{b1}(1P)\gamma$. The predicted partial decay widths are

$$\Gamma[h_b(1P) \rightarrow \chi_{b0}(1P)\gamma] = 9.4 \times 10^{-6} \text{ keV}, \quad (33)$$

$$\Gamma[h_b(1P) \rightarrow \chi_{b1}(1P)\gamma] = 9.0 \times 10^{-4} \text{ keV}. \quad (34)$$

Similar results are obtained in the framework of the relativized quark model [9] and nonrelativistic constituent quark model [10] (see Tab. III). These M1 transitions are so weak that we may hardly observe them in experiments.

D. Radiative transitions of $1D$ states

In the $1D$ bottomonium states, only the 2^{--} state $\Upsilon_2(1D)$ with a mass of $M_{\Upsilon_2(1D)} = 10164$ MeV is confirmed in experiments [50]. The other $1D$ states are still missing. The discovery of the $\Upsilon_2(1D)$ state provides a strong constrain of the mass of the other $1D$ states. Combining the predicted multiplet mass splittings with measured mass of $M_{\Upsilon_2(1D)} = 10164$ MeV, one can predict the masses for the $\Upsilon_1(1D)$, $\Upsilon_3(1D)$ and $\eta_{b2}(1D)$ states, which are $M_{\Upsilon_1(1D)} \simeq 10157$ MeV, $M_{\Upsilon_3(1D)} \simeq 10168$ MeV, and $M_{\eta_{b2}(1D)} \simeq 10164$ MeV, respectively.

1. $\Upsilon_2(1D)$

For the established 2^{--} state $\Upsilon_2(1D)$ [i.e., $\Upsilon_2(10164)$], the EM transitions are dominated by $\Upsilon_2(1D) \rightarrow \chi_{b1,2}(1P)\gamma$. The predicted partial decay widths are

$$\Gamma[\Upsilon_2(1D) \rightarrow \chi_{b1}(1P)\gamma] \simeq 21.8 \text{ keV}, \quad (35)$$

$$\Gamma[\Upsilon_2(1D) \rightarrow \chi_{b2}(1P)\gamma] \simeq 7.23 \text{ keV}, \quad (36)$$

and their ratio is

$$\frac{\Gamma[\Upsilon_2(1D) \rightarrow \chi_{b1}(1P)\gamma]}{\Gamma[\Upsilon_2(1D) \rightarrow \chi_{b2}(1P)\gamma]} \simeq 3.02. \quad (37)$$

Our results are in agreement with the predictions with the previous SNR potential model [8], relativistic quark model [13], and nonrelativistic constituent quark model [10]. The predicted partial width of $\Gamma[\Upsilon_2(1D) \rightarrow \chi_{b0}(1P)\gamma]$ is negligibly small. Some observations in the $\chi_{b1,2}(1P)\gamma$ channels are necessary to obtain more knowledge about $\Upsilon_2(1D)$.

2. The missing $1D$ states

Using the predicted mass $M_{\Upsilon_1(1D)} = 10157$ MeV for $\Upsilon_1(1D)$, we calculate the partial decay widths of $\Gamma[\Upsilon_1(1D) \rightarrow \chi_{b0,1,2}(1P)\gamma]$. Our results

$$\Gamma[\Upsilon_1(1D) \rightarrow \chi_{b0}(1P)\gamma] \simeq 19.8 \text{ keV}, \quad (38)$$

$$\Gamma[\Upsilon_1(1D) \rightarrow \chi_{b1}(1P)\gamma] \simeq 13.3 \text{ keV}, \quad (39)$$

$$\Gamma[\Upsilon_1(1D) \rightarrow \chi_{b2}(1P)\gamma] \simeq 1.02 \text{ keV}, \quad (40)$$

are consistent with those from the SNR potential model [8], relativistic quark model [13], and nonrelativistic constituent quark model [10] (see Tab. V). Our predictions show that the $\Upsilon_1(1D) \rightarrow \chi_{b0,1}(1P)\gamma$ might be good processes for the search for the missing $\Upsilon_1(1D)$ state.

While taking the mass of $\Upsilon_3(1D)$ with $M_{\Upsilon_3(1D)} = 10168$ MeV, we calculate the partial decay widths of $\Gamma[\Upsilon_3(1D) \rightarrow \chi_{b0,1,2}(1P)\gamma]$, our results are

$$\Gamma[\Upsilon_3(1D) \rightarrow \chi_{b0}(1P)\gamma] \simeq 9.2 \times 10^{-5} \text{ keV}, \quad (41)$$

$$\Gamma[\Upsilon_3(1D) \rightarrow \chi_{b1}(1P)\gamma] \simeq 1.1 \times 10^{-2} \text{ keV}, \quad (42)$$

$$\Gamma[\Upsilon_3(1D) \rightarrow \chi_{b2}(1P)\gamma] \simeq 32.1 \text{ keV}. \quad (43)$$

It is found that the EM decays of $\Upsilon_3(1D)$ are governed by the $\chi_{b2}(1P)\gamma$ channel, and the decay rates to the $\chi_{b0,1}(1P)\gamma$ channels are negligibly small. Our prediction of $\Gamma[\Upsilon_3(1D) \rightarrow \chi_{b2}(1P)\gamma] \simeq 32.1$ keV is consistent with the predictions from the potential models [8, 9] and relativistic quark model [13] (see Tab. V). To establish $\Upsilon_3(1D)$, the decay channel $\chi_{b2}(1P)\gamma$ is worth to observing in future experiments.

For the singlet $1D$ state $\eta_{b2}(1D)$, its mass is adopted as $M_{\eta_{b2}(1D)} = 10164$ MeV. We study the radiative transition $\eta_{b2}(1D) \rightarrow h_b(1P)\gamma$. Our predicted partial width is

$$\Gamma[\eta_{b2}(1D) \rightarrow h_b(1P)\gamma] \simeq 30.3 \text{ keV}, \quad (44)$$

which is close to the predictions from the other potential models [8, 9, 13] (see Tab. V). The large radiative transition rate indicates that the missing $\eta_{b2}(1D)$ state is most likely to be observed in the $h_b(1P)\gamma$ channel.

E. Radiative transitions of $2P$ states

1. $\chi_{b1}(2P)$

The $\chi_{b1}(2P)$ state can decay into $\Upsilon(1S, 2S)\gamma$, $\Upsilon(1^3D_{2,3})\gamma$ and $h_b(1P)\gamma$ via radiative transitions. Our predicted partial widths for the $\chi_{b1}(2P)$ decaying into the S -wave states

$\Upsilon(1S, 2S)$ are

$$\Gamma[\chi_{b1}(2P) \rightarrow \Upsilon(1S)\gamma] \simeq 11.7 \text{ keV}, \quad (45)$$

$$\Gamma[\chi_{b1}(2P) \rightarrow \Upsilon(2S)\gamma] \simeq 15.7 \text{ keV}, \quad (46)$$

which are consistent with observations from the CLEO Collaboration [51], and close to the other theoretical predictions (see Tab. IV). The branching ratio

$$\frac{\Gamma[\chi_{b1}(2P) \rightarrow \Upsilon(2S)\gamma]}{\Gamma[\chi_{b1}(2P) \rightarrow \Upsilon(1S)\gamma]} \simeq 1.34, \quad (47)$$

is slightly smaller than the world average value 2.2 ± 0.4 from the PDG [7]. From Tab. IV, we can find that this ratio has a strong model dependency. To test the predictions from various model, more accurate measurements are needed in experiments.

The decay rates of $\chi_{b1}(2P)$ into the D -wave states $\Upsilon_{1,2}(1D)$ are much weaker than those into the S -wave states. Our predictions are

$$\Gamma[\chi_{b1}(2P) \rightarrow \Upsilon_1(1D)\gamma] \simeq 0.56 \text{ keV}, \quad (48)$$

$$\Gamma[\chi_{b1}(2P) \rightarrow \Upsilon_2(1D)\gamma] \simeq 0.50 \text{ keV}, \quad (49)$$

which are close to the other model predictions [8–10, 13].

Furthermore, the typical M1 transition $\chi_{b2}(2P) \rightarrow h_b(1P)\gamma$ is also studied. The predicted partial decay width

$$\Gamma[\chi_{b2}(2P) \rightarrow h_b(1P)\gamma] \simeq 1.8 \times 10^{-4} \text{ keV}, \quad (50)$$

is about an order of magnitude smaller than the recent prediction $2.2 \times 10^{-3} \text{ keV}$ in Ref. [9]. However, the recent prediction $1.7 \times 10^{-4} \text{ keV}$ with a nonrelativistic constituent quark model [10] is in good agreement with our prediction. Lattice QCD study may be able to clarify this puzzle.

We expect more observations for the radiative transitions of $\chi_{b1}(2P)$ can be carried out to better understand the heavy quarkonium physics. If the $X(3872)$ resonance is confirmed as the $\chi_{c1}(2P)$ state, it is close to the threshold of $D\bar{D}$ and DD^* . However, the $\chi_{b1}(2P)$ state is far from the threshold of $B\bar{B}$ and BB^* . Thus, a combined study of the $\chi_{c1}(2P)$ and $\chi_{b1}(2P)$ should be helpful for us to understand the threshold effects in the heavy quarkonium states.

2. $\chi_{b2}(2P)$

The $\chi_{b2}(2P)$ state can decay into $\Upsilon(1S, 2S)\gamma$, $\Upsilon_{1,2,3}(1D)\gamma$ and $h_b(1P)\gamma$ channels. In these decays, the $\chi_{b2}(2P) \rightarrow \Upsilon(1S, 2S)\gamma$ processes play dominant roles. We predict that

$$\Gamma[\chi_{b2}(2P) \rightarrow \Upsilon(1S)\gamma] \simeq 13.6 \text{ keV}, \quad (51)$$

$$\Gamma[\chi_{b2}(2P) \rightarrow \Upsilon(2S)\gamma] \simeq 15.7 \text{ keV}, \quad (52)$$

which is close to the other model predictions [8–10, 13], and compatible with the observations from the CLEO Collaboration [51] (see Tab. IV). According to these predicted partial widths, we estimate the partial width ratio:

$$\frac{\Gamma[\chi_{b2}(2P) \rightarrow \Upsilon(2S)\gamma]}{\Gamma[\chi_{b2}(2P) \rightarrow \Upsilon(1S)\gamma]} \simeq 1.15, \quad (53)$$

which is close to the lower limit of the world average data $1.51^{+0.59}_{-0.47}$ from the PDG [7]. For this ratio, there are strong model dependencies. Thus, more accurate measurements are needed to test various model predictions.

The decay rates of $\chi_{b2}(2P) \rightarrow \Upsilon_{1,2,3}(1D)\gamma$ are much weaker than those of $\chi_{b2}(2P) \rightarrow \Upsilon(1S, 2S)\gamma$. Our predicted results are

$$\Gamma[\chi_{b2}(2P) \rightarrow \Upsilon_1(1D)\gamma] \simeq 0.026 \text{ keV}, \quad (54)$$

$$\Gamma[\chi_{b2}(2P) \rightarrow \Upsilon_2(1D)\gamma] \simeq 0.42 \text{ keV}, \quad (55)$$

$$\Gamma[\chi_{b2}(2P) \rightarrow \Upsilon_3(1D)\gamma] \simeq 2.51 \text{ keV}, \quad (56)$$

which are in compatible with the predictions in Refs. [8, 10, 13] (see Tab. IV). The weak decay rate indicates that the productions of $1D$ -wave states $\Upsilon(1^3D_{1,2,3})\gamma$ are hard through the EM decays of $\chi_{b2}(2P)$.

3. $h_b(2P)$

The $h_b(2P)$ state can decay into $\eta_b(1S, 2S)\gamma$, $\eta_{b2}(1D)\gamma$, and $\chi_{b0,1,2}(1P)\gamma$ via EM transitions, in which the $\eta_b(1S, 2S)\gamma$ decay modes are dominant. We calculate the partial decay widths of $\Gamma[h_b(2P) \rightarrow \eta_b(1S, 2S)\gamma]$. Our results are

$$\Gamma[h_b(2P) \rightarrow \eta_b(1S)\gamma] \simeq 17.5 \text{ keV}, \quad (57)$$

$$\Gamma[h_b(2P) \rightarrow \eta_b(2S)\gamma] \simeq 16.6 \text{ keV}, \quad (58)$$

which is compatible with the calculations from the other models [8–10, 13]. Our predicted partial width ratio

$$\frac{\Gamma[h_b(2P) \rightarrow \eta_b(2S)\gamma]}{\Gamma[h_b(2P) \rightarrow \eta_b(1S)\gamma]} \simeq 0.95, \quad (59)$$

is close to lower limit of the measurement 2.5 ± 1.2 from the Belle Collaboration [52]. To test the various model predictions, more accurate measurements of the ratio are needed.

We also calculate the partial decay width of $\Gamma[h_b(2P) \rightarrow \eta_{b2}(1D)\gamma]$. Our result is

$$\Gamma[h_b(2P) \rightarrow \eta_{b2}(1D)\gamma] \simeq 2.24 \text{ keV}, \quad (60)$$

which is compatible with the predictions from the relativized quark model [9] and the relativistic quark model [13].

Finally, we give our predictions for the typical M1 transitions $h_b(2P) \rightarrow \chi_{b0,1,2}(1P)\gamma$. The predicted results

$$\Gamma[h_b(2P) \rightarrow \chi_{b0}(1P)\gamma] \simeq 10.0 \text{ keV}, \quad (61)$$

$$\Gamma[h_b(2P) \rightarrow \chi_{b1}(1P)\gamma] \simeq 2.5 \text{ keV}, \quad (62)$$

$$\Gamma[h_b(2P) \rightarrow \chi_{b2}(1P)\gamma] \simeq 1.1 \text{ keV}. \quad (63)$$

About these M1 transitions, there are obvious differences in various model predictions (see Tab. III).

F. Radiative transitions of $3S$ states

1. $\Upsilon(3S)$

$\Upsilon(3S)$ is well-established in experiments. Its mass and width are $M_{\Upsilon(3S)} = 10355.2 \pm 0.5 \text{ MeV}$ and $\Gamma = 20.32 \pm 1.85$

keV, respectively. The EM transitions $\Upsilon(3S) \rightarrow \chi_{bJ}(1P, 2P)\gamma$ and $\Upsilon(3S) \rightarrow \eta_b(1S, 2S)\gamma$ have been observed in experiments.

For the EM transitions $\Upsilon(3S) \rightarrow \chi_{bJ}(1P)\gamma$, the predicted partial widths are

$$\Gamma[\Upsilon(3S) \rightarrow \chi_{b0}(1P)\gamma] \simeq 0.097 \text{ keV}, \quad (64)$$

$$\Gamma[\Upsilon(3S) \rightarrow \chi_{b1}(1P)\gamma] \simeq 0.0005 \text{ keV}, \quad (65)$$

$$\Gamma[\Upsilon(3S) \rightarrow \chi_{b2}(1P)\gamma] \simeq 0.14 \text{ keV}, \quad (66)$$

which are compatible with the world average data from the PDG [7]. Compared with the previous SNR model calculations in Ref. [8], our results are more close to the measurements. It indicates that the corrections of the spin-dependent interactions to the wavefunctions are important to understand these EM transitions, which was also found in Ref. [53]. About these transitions, the predictions in various models are very different. More model-independent studies are needed in theory.

While for the EM transitions $\Upsilon(3S) \rightarrow \chi_{bJ}(2P)\gamma$, we predict that

$$\Gamma[\Upsilon(3S) \rightarrow \chi_{b0}(2P)\gamma] \simeq 1.21 \text{ keV}, \quad (67)$$

$$\Gamma[\Upsilon(3S) \rightarrow \chi_{b1}(2P)\gamma] \simeq 2.61 \text{ keV}, \quad (68)$$

$$\Gamma[\Upsilon(3S) \rightarrow \chi_{b2}(2P)\gamma] \simeq 3.16 \text{ keV}, \quad (69)$$

which are in good agreement with the experimental data and the predictions in [8–13].

For the typical M1 transitions $\Upsilon(3S) \rightarrow \eta_b(1S, 2S)\gamma$, the predicted partial widths are

$$\Gamma[\Upsilon(3S) \rightarrow \eta_b(1S)\gamma] \simeq 71 \text{ eV}, \quad (70)$$

$$\Gamma[\Upsilon(3S) \rightarrow \eta_b(2S)\gamma] \simeq 11 \text{ eV}, \quad (71)$$

which are the same order of magnitude as the predictions from the recent nonrelativistic constituent quark model [10]. However, our prediction of the $\Gamma[\Upsilon(3S) \rightarrow \eta_b(1S)\gamma] \simeq 71 \text{ eV}$ is notably larger than the world average data $10 \pm 2 \text{ eV}$ [7]. To clarify this puzzle, more studies are needed.

2. $\eta_b(3S)$

The 3^1S_0 bottomonium state, $\eta_b(3S)$, is still missing. The predicted mass splitting between 3^3S_1 and 3^1S_0 is about 17 MeV. Combined with the measured mass of 3^3S_1 , the mass of $\eta_b(3S)$ might be $M_{\eta_b(3S)} \simeq 10338 \text{ MeV}$. Using this predicted mass, we study the E1 transitions $\eta_b(3S) \rightarrow h_b(1P, 2P)\gamma$ and M1 transitions $\eta_b(3S) \rightarrow \Upsilon(1S, 2S)\gamma$.

For the E1 transitions $\eta_b(3S) \rightarrow h_b(1P, 2P)\gamma$, our predicted partial widths are

$$\Gamma[\eta_b(3S) \rightarrow h_b(1P)\gamma] \simeq 0.67 \text{ keV}, \quad (72)$$

$$\Gamma[\eta_b(3S) \rightarrow h_b(2P)\gamma] \simeq 4.25 \text{ keV}. \quad (73)$$

With the corrections of the spin-dependent potentials to the wavefunctions, our results are about a factor 2 smaller than the previous SNR₀ model predictions [8]. While, our predictions are about a factor 2 larger than those from the relativistic

quark model [13] (see Tab. IV). It should be mentioned that our predicted partial width ratio

$$\frac{\Gamma[\eta_b(3S) \rightarrow h_b(2P)\gamma]}{\Gamma[\eta_b(3S) \rightarrow h_b(1P)\gamma]} \simeq 6.1. \quad (74)$$

is notably different from the other model predictions [8–10, 13], which is expected to be measured in future experiments.

While for the M1 transitions $\eta_b(3S) \rightarrow \Upsilon(1S, 2S)\gamma$, our predicted partial widths are

$$\Gamma[\eta_b(3S) \rightarrow \Upsilon(1S)\gamma] \simeq 6.0 \times 10^{-2} \text{ keV}, \quad (75)$$

$$\Gamma[\eta_b(3S) \rightarrow \Upsilon(2S)\gamma] \simeq 8.7 \times 10^{-3} \text{ keV}, \quad (76)$$

which are in compatible with the recent predictions in Refs. [9, 10], however, about a factor 3 larger than the predictions with the relativistic quark model [13]. These M1 transitions should be further studied in theory.

G. Radiative transitions of $2D$ states

Until now, no $2D$ bottomonium states have been observed in experiments. In the calculations, their masses are adopted from our potential model predictions.

1. $\Upsilon_3(2D)$

The radiative transitions of $\Upsilon_3(2D)$ are dominated by the $\chi_{b2}(2P)\gamma$ channel, the partial widths decaying into $\chi_{b2}(1P)\gamma$ channels are also sizeable. Taking the mass of $M_{\Upsilon_3(2D)} = 10436 \text{ MeV}$ predicted by us, we obtain

$$\Gamma[\Upsilon_3(2D) \rightarrow \chi_{b2}(2P)\gamma] \simeq 17.0 \text{ keV}, \quad (77)$$

$$\Gamma[\Upsilon_3(2D) \rightarrow \chi_{b2}(1P)\gamma] \simeq 5.22 \text{ keV}. \quad (78)$$

Our predictions are roughly close to those of other models [8–10, 13] (see Tab. V). Our predicted partial width ratio

$$\frac{\Gamma[\Upsilon_3(2D) \rightarrow \chi_{b2}(2P)\gamma]}{\Gamma[\Upsilon_3(2D) \rightarrow \chi_{b2}(1P)\gamma]} = 3.3, \quad (79)$$

is compatible with the recent prediction ~ 2.8 from the non-relativistic constituent quark model [10].

2. $\Upsilon_2(2D)$

The radiative transitions of $\Upsilon_2(2D)$ are dominated by the $\chi_{b1}(2P)\gamma$ channel, the partial widths decaying into $\chi_{b2}(2P)\gamma$, $\chi_{b1}(1P)\gamma$ and $\chi_{b2}(1P)\gamma$ channels are also sizeable. With the predicted mass $M_{\Upsilon_2(2D)} = 10432 \text{ MeV}$, we predict the partial widths:

$$\Gamma[\Upsilon_2(2D) \rightarrow \chi_{b1}(2P)\gamma] \simeq 11.4 \text{ keV}, \quad (80)$$

$$\Gamma[\Upsilon_2(2D) \rightarrow \chi_{b2}(2P)\gamma] \simeq 3.75 \text{ keV}, \quad (81)$$

$$\Gamma[\Upsilon_2(2D) \rightarrow \chi_{b1}(1P)\gamma] \simeq 4.00 \text{ keV}, \quad (82)$$

$$\Gamma[\Upsilon_2(2D) \rightarrow \chi_{b2}(1P)\gamma] \simeq 1.11 \text{ keV}, \quad (83)$$

and the partial width ratios:

$$\frac{\Gamma[\Upsilon_2(2D) \rightarrow \chi_{b1}(2P)\gamma]}{\Gamma[\Upsilon_2(2D) \rightarrow \chi_{b2}(2P)\gamma]} \simeq 3.0, \quad (84)$$

$$\frac{\Gamma[\Upsilon_2(2D) \rightarrow \chi_{b1}(1P)\gamma]}{\Gamma[\Upsilon_2(2D) \rightarrow \chi_{b2}(1P)\gamma]} \simeq 3.6. \quad (85)$$

Our predictions for the partial widths are comparable with the other model predictions in magnitude [8–10, 13]. However, the predicted ratios from different models are very different (see Tab. V).

3. $\Upsilon_1(2D)$

The radiative transitions of $\Upsilon_1(2D)$ are dominated by the $\chi_{b0,1}(2P)\gamma$ channels, the partial widths decaying into $\chi_{b0,1,2}(1P)\gamma$ and $\chi_{b2}(2P)\gamma$ channels are also sizeable. Taking the mass of $M_{\Upsilon_1(2D)} = 10425$ MeV, we calculate the partial decay widths. Our predicted partial widths for the transitions $\Upsilon_1(2D) \rightarrow \chi_{b0,1,2}(2P)\gamma$ are

$$\Gamma[\Upsilon_1(2D) \rightarrow \chi_{b0}(2P)\gamma] \simeq 9.58 \text{ keV}, \quad (86)$$

$$\Gamma[\Upsilon_1(2D) \rightarrow \chi_{b1}(2P)\gamma] \simeq 6.74 \text{ keV}, \quad (87)$$

$$\Gamma[\Upsilon_1(2D) \rightarrow \chi_{b2}(2P)\gamma] \simeq 0.47 \text{ keV}. \quad (88)$$

These predictions are consistent with the other potential predictions in magnitude [8–10, 13] (see Tab. V). Furthermore, our predicted partial width ratio

$$\frac{\Gamma[\Upsilon_1(2D) \rightarrow \chi_{b0}(2P)\gamma]}{\Gamma[\Upsilon_1(2D) \rightarrow \chi_{b1}(2P)\gamma]} = 1.4, \quad (89)$$

is also close to the value $1.5 \sim 1.9$ obtained from the other potential models [8–10, 13].

Our predicted partial widths for the transitions $\Upsilon_1(2D) \rightarrow \chi_{b0,1,2}(1P)\gamma$ are

$$\Gamma[\Upsilon_1(2D) \rightarrow \chi_{b0}(1P)\gamma] \simeq 5.56 \text{ keV}, \quad (90)$$

$$\Gamma[\Upsilon_1(2D) \rightarrow \chi_{b1}(1P)\gamma] \simeq 2.17 \text{ keV}, \quad (91)$$

$$\Gamma[\Upsilon_1(2D) \rightarrow \chi_{b2}(1P)\gamma] \simeq 0.44 \text{ keV}. \quad (92)$$

Our predicted partial widths for the transitions $\Upsilon_2(2D) \rightarrow \chi_{b0,1}(1P)\gamma$ roughly agree with those from the SNR_1 model [8] and nonrelativistic constituent quark model [10]. From Tab. V, one can see that the $\Gamma[\Upsilon_2(2D) \rightarrow \chi_{b2}(1P)\gamma]$ predicted in various models is very different.

4. $\eta_{b2}(2D)$

The main EM decay channels of $\eta_{b2}(2D)$ (i.e., $\eta_{b2}(2^1D_2)$) are $h_b(2P)\gamma$ and $h_b(1P)\gamma$. With the mass $M_{\eta_{b2}(2D)} = 10432$ MeV predicted by us, the partial widths of the transitions $\eta_{b2}(2D) \rightarrow h_b(1P, 2P)\gamma$ might be

$$\Gamma[\eta_{b2}(2D) \rightarrow h_b(1P)\gamma] \simeq 5.66 \text{ keV}, \quad (93)$$

$$\Gamma[\eta_{b2}(2D) \rightarrow h_b(2P)\gamma] \simeq 15.6 \text{ keV}, \quad (94)$$

which roughly agree with the potential models predictions [8–10]. Our predicted partial width ratio

$$\frac{\Gamma[\eta_{b2}(2D) \rightarrow h_b(2P)\gamma]}{\Gamma[\eta_{b2}(2D) \rightarrow h_b(1P)\gamma]} = 2.7, \quad (95)$$

is in good agreement with the recent prediction 2.8 in the non-relativistic constituent quark model [10].

As a whole, the EM decay rates of $2D \rightarrow 1P, 2P$ are sizeable, to determine these $2D$ states in experiments, their transitions into the $1P$ and $2P$ states are worth observing.

H. Radiative transitions of $3P$ states

In the past several years, great progress has been achieved in the observations of the $3P$ bottomonium states. In 2011, the ATLAS Collaboration first discovered the $\chi_b(3P)$ through its radiative transitions to $\Upsilon(1S, 2S)$ with $\Upsilon(1S, 2S) \rightarrow \mu^+\mu^-$ at the LHC [54]. Only a few months after that, the $\chi_b(3P)$ state was confirmed by the D0 Collaboration [55]. Recently, the LHCb Collaboration also carried out a precise measurement of the $\chi_b(3P)$ state, they identified $\chi_b(3P)$ as the $\chi_{b1}(3P)$ state [56, 57]. The measured mass of $\chi_{b1}(3P)$ is $M_{\chi_{b1}(3P)} = 10516$ MeV. Combined the predicted mass splittings between the $3P$ states with the measured mass of $\chi_{b1}(3P)$, the estimated masses of $\chi_{b2}(3P)$, $\chi_{b0}(3P)$ and $h_b(3P)$ are $M_{\chi_{b2}(3P)} \simeq 10529$ MeV, $M_{\chi_{b0}(3P)} \simeq 10491$ MeV, and $M_{h_b(3P)} \simeq 10520$ MeV, respectively.

1. $\chi_{b1}(3P)$

The $\Upsilon(1S, 2S, 3S)\gamma$ are the main EM decay channels of $\chi_{b1}(3P)$. Our predicted partial widths for these channels are

$$\Gamma[\chi_{b1}(3P) \rightarrow \Upsilon(1S)\gamma] \simeq 6.41 \text{ keV}, \quad (96)$$

$$\Gamma[\chi_{b1}(3P) \rightarrow \Upsilon(2S)\gamma] \simeq 5.63 \text{ keV}, \quad (97)$$

$$\Gamma[\chi_{b1}(3P) \rightarrow \Upsilon(3S)\gamma] \simeq 10.3 \text{ keV}. \quad (98)$$

They are close to the recent calculations with the nonrelativistic constituent quark model [10], and the predictions with the previous SNR potential models [8]. Our predicted partial width ratio

$$\frac{\Gamma[\chi_{b1}(3P) \rightarrow \Upsilon(2S)\gamma]}{\Gamma[\chi_{b1}(3P) \rightarrow \Upsilon(1S)\gamma]} \simeq 0.88, \quad (99)$$

is in agreement with the predictions from the SNR_0 model [8] and nonrelativistic constituent quark model [10]. And

$$\frac{\Gamma[\chi_{b1}(3P) \rightarrow \Upsilon(3S)\gamma]}{\Gamma[\chi_{b1}(3P) \rightarrow \Upsilon(2S)\gamma]} \simeq 1.8 \quad (100)$$

predicted by us are also compatible with the predictions $2.0 \sim 3.0$ from the potential models [8–10].

Taking the masses of $2D$ waves calculated by us, we predict that

$$\Gamma[\chi_{b1}(3P) \rightarrow \Upsilon_1(2D)\gamma] \simeq 1.07 \text{ keV}, \quad (101)$$

$$\Gamma[\chi_{b1}(3P) \rightarrow \Upsilon_2(2D)\gamma] \simeq 0.94 \text{ keV}. \quad (102)$$

Our results are close to the potential model predictions [8, 9]. The sizeable partial widths of $\Gamma[\chi_{b1}(3P) \rightarrow \Upsilon_{1,2}(2D)\gamma]$ indicate one may discover the missing D -wave states $\Upsilon_1(2D)$ and $\Upsilon_2(2D)$ through the radiative transitions $\chi_{b1}(3P) \rightarrow \Upsilon_{1,2}(2D)\gamma$.

The radiative decay rates of $\chi_{b1}(3P)$ into the $1D$ -wave states are too small to compare with that into the S -, and $2D$ -wave states. Our results are listed in Tab. IV. These decay modes may be hardly observed in experiments.

2. $\chi_{b2}(3P)$

With $M_{\chi_{b2}(3P)} = 10529$ MeV for the $\chi_{b2}(3P)$ state, we calculate its radiative decay properties. Our results are listed in Tab. IV. It is found that radiative decay ratios of $\chi_{b2}(3P)$ into the $1D$ -wave states are negligibly small. While the partial widths for the transitions $\chi_{b2}(3P) \rightarrow \Upsilon(1S, 2S, 3S)\gamma$ and $\chi_{b1}(3P) \rightarrow \Upsilon_3(2D)\gamma$ are sizeable. Taking the masses of $2D$ -wave states predicted by us, we have

$$\Gamma[\chi_{b2}(3P) \rightarrow \Upsilon_3(2D)\gamma] \simeq 4.60 \text{ keV}, \quad (103)$$

$$\Gamma[\chi_{b2}(3P) \rightarrow \Upsilon_2(2D)\gamma] \simeq 0.78 \text{ keV}, \quad (104)$$

$$\Gamma[\chi_{b2}(3P) \rightarrow \Upsilon_1(2D)\gamma] \simeq 0.049 \text{ keV}, \quad (105)$$

which are consistent with the previous SNR potential model calculations [8].

And our predicted partial widths

$$\Gamma[\chi_{b2}(3P) \rightarrow \Upsilon(1S)\gamma] \simeq 8.17 \text{ keV}, \quad (106)$$

$$\Gamma[\chi_{b2}(3P) \rightarrow \Upsilon(2S)\gamma] \simeq 6.72 \text{ keV}, \quad (107)$$

$$\Gamma[\chi_{b2}(3P) \rightarrow \Upsilon(3S)\gamma] \simeq 10.8 \text{ keV}, \quad (108)$$

are consistent with the previous SNR potential model calculations as well [8]. Combing the predicted partial widths with each other, we easily obtain their ratios:

$$\frac{\Gamma[\chi_{b2}(3P) \rightarrow \Upsilon(2S)\gamma]}{\Gamma[\chi_{b2}(3P) \rightarrow \Upsilon(1S)\gamma]} \simeq 0.82, \quad (109)$$

$$\frac{\Gamma[\chi_{b2}(3P) \rightarrow \Upsilon(3S)\gamma]}{\Gamma[\chi_{b2}(3P) \rightarrow \Upsilon(2S)\gamma]} \simeq 1.6. \quad (110)$$

These ratios for $\chi_{b2}(2P)$ decaying into the S -wave states are very similar to the corresponding ratios of $\chi_{b1}(2P)$, which is expected to be tested by future experiments.

3. $\chi_{b0}(3P)$

With the predicted mass $M_{\chi_{b0}(3P)} = 10491$ MeV for the $\chi_{b0}(3P)$ state, we calculate its radiative decay properties. Our results are listed in Tab. IV. It is found that the partial radiative decay widths of $\chi_{b0}(3P)$ into the S -wave states $\Upsilon(1S, 2S, 3S)$ are comparable to those of $\chi_{b1,2}(3P)$. Our predicted partial widths

$$\Gamma[\chi_{b0}(3P) \rightarrow \Upsilon(1S)\gamma] \simeq 1.87 \text{ keV}, \quad (111)$$

$$\Gamma[\chi_{b0}(3P) \rightarrow \Upsilon(2S)\gamma] \simeq 2.55 \text{ keV}, \quad (112)$$

$$\Gamma[\chi_{b0}(3P) \rightarrow \Upsilon(3S)\gamma] \simeq 7.95 \text{ keV}, \quad (113)$$

and ratios

$$\frac{\Gamma[\chi_{b0}(3P) \rightarrow \Upsilon(2S)\gamma]}{\Gamma[\chi_{b0}(3P) \rightarrow \Upsilon(1S)\gamma]} \simeq 1.4, \quad (114)$$

$$\frac{\Gamma[\chi_{b0}(3P) \rightarrow \Upsilon(3S)\gamma]}{\Gamma[\chi_{b0}(3P) \rightarrow \Upsilon(2S)\gamma]} \simeq 3.1, \quad (115)$$

are in good agreement with the recent calculations with the nonrelativistic constituent quark model [10].

For the partial decay widths $\Gamma[\chi_{b0}(3P) \rightarrow \Upsilon(1D, 2D)\gamma]$, our predictions are

$$\Gamma[\chi_{b0}(3P) \rightarrow \Upsilon_1(1D)\gamma] \simeq 0.15 \text{ keV}, \quad (116)$$

$$\Gamma[\chi_{b0}(3P) \rightarrow \Upsilon_1(2D)\gamma] \simeq 2.20 \text{ keV}, \quad (117)$$

which are close to the recent predictions with the GI model [9].

4. $h_b(3P)$

For the singlet $h_b(3P)$ state, with the predicted mass $M_{h_b(3P)} = 10520$ MeV we calculate its radiative decay properties. Our results are listed in Tab. IV. The EM decays of $h_b(3P)$ are dominated by the $\eta_b(3S)\gamma$ channel, while the partial widths into the $\eta_b(1S, 2S)\gamma$ and $\eta_{b2}(2D)\gamma$ channels are sizeable as well. Our predicted partial decay widths into the S -wave states,

$$\Gamma[h_b(3P) \rightarrow \eta_b(1S)\gamma] \simeq 10.7 \text{ keV}, \quad (118)$$

$$\Gamma[h_b(3P) \rightarrow \eta_b(2S)\gamma] \simeq 7.63 \text{ keV}, \quad (119)$$

$$\Gamma[h_b(3P) \rightarrow \eta_b(3S)\gamma] \simeq 14.1 \text{ keV}, \quad (120)$$

are the same order of those from various potential models [8–10] (see Tab. IV). Combing the predicted partial widths with each other, we easily obtain their ratios:

$$\frac{\Gamma[h_b(3P) \rightarrow \eta_b(2S)\gamma]}{\Gamma[h_b(3P) \rightarrow \eta_b(1S)\gamma]} \simeq 0.71, \quad (121)$$

$$\frac{\Gamma[h_b(3P) \rightarrow \eta_b(3S)\gamma]}{\Gamma[h_b(3P) \rightarrow \eta_b(2S)\gamma]} \simeq 1.8. \quad (122)$$

Form Tab. IV, we find that there is a strong model dependency in these ratios.

Furthermore, we calculate the partial decay widths into the D -wave states. Our results are

$$\Gamma[h_b(3P) \rightarrow \eta_{b2}(1D)\gamma] \simeq 0.18 \text{ keV}, \quad (123)$$

$$\Gamma[h_b(3P) \rightarrow \eta_{b2}(2D)\gamma] \simeq 4.21 \text{ keV}, \quad (124)$$

which are close to the recent predictions with the nonrelativistic constituent quark model [10].

As a whole, to look for the missing $3P$ states, their EM transitions into the $1S, 2S$ and $3S$ final states are worth observing in experiments. Furthermore, some missing $2D$ -wave states $\Upsilon_j(2D)$ might be produced through the radiative transitions $\chi_b(3P) \rightarrow \Upsilon(2D)\gamma$.

IV. SUMMARY

In the nonrelativistic screened potential quark model framework, we study the bottomonium spectrum. The radial Schrödinger equation are solved with the three-point difference central method, where the spin-dependent potentials are dealt with non-perturbatively. In our calculations, the corrections of the spin-dependent interactions to the wavefunctions are successfully included as well. It is found that the corrections of spin-dependent interactions to the wavefunctions of the S -wave and $^3P_{0,1}$ states are notably. The bottomonium spectrum predicted within our approach is in a global agreement with the experimental data.

Moreover, using these wavefunctions we study the electromagnetic transitions of nS , nP ($n \leq 3$), and nD ($n \leq 2$) bottomonium states with a nonrelativistic electromagnetic transition operator widely applied to meson photoproduction reactions, in which the effects of binding potential between quarks is considered, and the possible higher EM multipole contribu-

tions are included. We obtain a reasonable description of the measured decay rates, except for some M1 transitions. Additionally, our predictions of the masses and unmeasured decay rates for some higher bottomonium states are also presented.

The LHC and Belle experiments have demonstrated the ability to observe and measure the properties of bottomonium mesons. In near future, more missing bottomonium states will be discovered and more decay channels will be measured in experiments. We expect that our theoretical predictions in this paper will be helpful for experimental exploration of the bottomonium mesons.

Acknowledgement

This work is supported, in part, by the National Natural Science Foundation of China (Grants No. 11075051 and No. 11375061), and the Hunan Provincial Natural Science Foundation (Grant No. 13JJ1018).

-
- [1] S. Godfrey and N. Isgur, Mesons in a Relativized Quark Model with Chromodynamics, *Phys. Rev. D* **32**, 189 (1985).
- [2] A. Garmash, Bottomonium Studies at Belle, *EPJ Web Conf.* **96**, 01014 (2015).
- [3] E. Eichten, S. Godfrey, H. Mahlke and J. L. Rosner, Quarkonia and their transitions, *Rev. Mod. Phys.* **80**, 1161 (2008) [hep-ph/0701208].
- [4] N. Brambilla *et al.* [Quarkonium Working Group Collaboration], Heavy quarkonium physics, hep-ph/0412158.
- [5] N. Brambilla *et al.*, Heavy quarkonium: progress, puzzles, and opportunities, *Eur. Phys. J. C* **71**, 1534 (2011) [arXiv:1010.5827 [hep-ph]].
- [6] A. J. Bevan *et al.* [BaBar and Belle Collaborations], The Physics of the B Factories, *Eur. Phys. J. C* **74**, 3026 (2014) [arXiv:1406.6311 [hep-ex]].
- [7] K. A. Olive *et al.* [Particle Data Group Collaboration], Review of Particle Physics, *Chin. Phys. C* **38**, 090001 (2014).
- [8] B. Q. Li and K. T. Chao, Bottomonium Spectrum with Screened Potential, *Commun. Theor. Phys.* **52**, 653 (2009) [arXiv:0909.1369 [hep-ph]].
- [9] S. Godfrey and K. Moats, Bottomonium Mesons and Strategies for Their Observation, arXiv:1507.00024 [hep-ph].
- [10] J. Segovia, P. G. Ortega, D. R. Entem and F. Fernández, Bottomonium spectrum revisited, *Phys. Rev. D* **93**, 074027 (2016)
- [11] A. Barducci, R. Giachetti and E. Sorace, arXiv:1604.08043 [hep-ph].
- [12] Wei-Zhao Tian, Lu Cao, You-Chang Yang and Hong Chen, Bottomonium states versus recent experimental observations in the QCD-inspired potential model, *Chin. Phys. C* **37**, 083101 (2013) [arXiv:1308.0960 [hep-ph]].
- [13] D. Ebert, R. N. Faustov and V. O. Galkin, Properties of heavy quarkonia and B_c mesons in the relativistic quark model, *Phys. Rev. D* **67**, 014027 (2003) [hep-ph/0210381].
- [14] N. Akbar, M. A. Sultan, B. Masud and F. A. Sultan, Higher Hybrid Bottomonia in an Extended Potential Model, arXiv:1511.03632 [hep-ph].
- [15] C. Hughes, R. J. Dowdall, C. T. H. Davies, R. R. Horgan, G. von Hippel and M. Wingate, The Hindered M1 Radiative Decay $\Upsilon(2S) \rightarrow \eta_b(1S)\gamma$ from Lattice NRQCD, arXiv:1508.01694 [hep-lat].
- [16] R. Lewis and R. M. Woloshyn, Excited Upsilon Radiative Decays, *Phys. Rev. D* **84**, 094501 (2011) [arXiv:1108.1137 [hep-lat]].
- [17] D. Becirevi, M. Kruse and F. Sanfilippo, Lattice QCD estimate of the $\eta_c(2S) \rightarrow J/\psi\gamma$ decay rate, *JHEP* **1505**, 014 (2015) [arXiv:1411.6426 [hep-lat]].
- [18] M. Baker, A. A. Penin, D. Seidel and N. Zerf, Bottomonium Hyperfine Splitting on the Lattice and in the Continuum, *Phys. Rev. D* **92**, 054502 (2015) [arXiv:1504.05979 [hep-ph]].
- [19] F. De Fazio, Radiative transitions of heavy quarkonium states, *Phys. Rev. D* **79**, 054015 (2009) [*Phys. Rev. D* **83**, 099901 (2011)] [arXiv:0812.0716 [hep-ph]].
- [20] N. Brambilla, Y. Jia and A. Vairo, Model-independent study of magnetic dipole transitions in quarkonium, *Phys. Rev. D* **73**, 054005 (2006) [hep-ph/0512369].
- [21] N. Brambilla, P. Pietrulewicz and A. Vairo, Model-independent Study of Electric Dipole Transitions in Quarkonium, *Phys. Rev. D* **85**, 094005 (2012) [arXiv:1203.3020 [hep-ph]].
- [22] A. Pineda and J. Segovia, Improved determination of heavy quarkonium magnetic dipole transitions in potential nonrelativistic QCD, *Phys. Rev. D* **87**, 074024 (2013) [arXiv:1302.3528 [hep-ph]].
- [23] J. Ferretti and E. Santopinto, Higher mass bottomonia, *Phys. Rev. D* **90**, 094022 (2014) [arXiv:1306.2874 [hep-ph]].
- [24] Y. Lu, M. N. Anwar and B. S. Zou, Coupled-Channel Effects for the Bottomonium with Realistic Wave Functions, arXiv:1606.06927 [hep-ph].
- [25] H. M. Choi, Decay constants and radiative decays of heavy mesons in light-front quark model, *Phys. Rev. D* **75**, 073016 (2007) [hep-ph/0701263].
- [26] H. W. Ke, X. Q. Li, Z. T. Wei and X. Liu, Re-Study on the wave functions of $\Upsilon(nS)$ states in LFQM and the radiative decays of $\Upsilon(nS) \rightarrow \eta_b\gamma$, *Phys. Rev. D* **82**, 034023 (2010) [arXiv:1006.1091 [hep-ph]].
- [27] H. W. Ke, X. Q. Li and X. Liu, Study on the Radiative Decays of $\Upsilon(nS) \rightarrow \eta_b\gamma$, arXiv:1002.1187 [hep-ph].

- [28] H. W. Ke, X. Q. Li and Y. L. Shi, The radiative decays of 0^{++} and 1^{+-} heavy mesons, *Phys. Rev. D* **87**, 054022 (2013) [arXiv:1301.4014 [hep-ph]].
- [29] B. Q. Li and K. T. Chao, Higher Charmonia and X,Y,Z states with Screened Potential, *Phys. Rev. D* **79**, 094004 (2009) [arXiv:0903.5506 [hep-ph]].
- [30] K.T. Chao and J.H. Liu, in Proceedings of the Workshop on Weak Interactions and CP Violation, Beijing, August 22-26, 1989, edited by T. Huang and D.D. Wu, World Scientific (Singapore, 1990) p.109-p.117.
- [31] Y. B. Ding, K. T. Chao and D. H. Qin, Screened $Q\bar{Q}$ potential and spectrum of heavy quarkonium, *Chin. Phys. Lett.* **10**, 460 (1993).
- [32] E. Laermann, F. Langhammer, I. Schmitt and P. M. Zerwas, The Interquark Potential: SU(2) Color Gauge Theory With Fermions, *Phys. Lett. B* **173**, 437 (1986).
- [33] K. D. Born, E. Laermann, N. Pirch, T. F. Walsh and P. M. Zerwas, Hadron Properties in Lattice QCD With Dynamical Fermions, *Phys. Rev. D* **40**, 1653 (1989). doi:10.1103/PhysRevD.40.1653
- [34] W. J. Deng, L. Y. Xiao, L. C. Gui and X. H. Zhong, Radiative transitions of charmonium states, arXiv:1510.08269 [hep-ph].
- [35] Z. P. Li, The Kaon photoproduction of nucleons in the chiral quark model, *Phys. Rev. C* **52**, 1648 (1995) [hep-ph/9502218].
- [36] Z. P. Li, H. X. Ye and M. H. Lu, An unified approach to pseudoscalar meson photoproductions off nucleons in the quark model, *Phys. Rev. C* **56**, 1099 (1997) [arXiv:nucl-th/9706010].
- [37] Q. Zhao, Eta-prime photoproduction near threshold, *Phys. Rev. C* **63**, 035205 (2001).
- [38] B. Saghai and Z. p. Li, Quark model study of the eta photoproduction: Evidence for a new S(11) resonance?, *Eur. Phys. J. A* **11**, 217 (2001) [nucl-th/0104084].
- [39] Q. Zhao, J. S. Al-Khalili, Z. P. Li and R. L. Workman, Pion photoproduction on the nucleon in the quark model, *Phys. Rev. C* **65**, 065204 (2002) [nucl-th/0202067].
- [40] J. He, B. Saghai and Z. Li, Study of η photoproduction on the proton in a chiral constituent quark approach via one-gluon-exchange model, *Phys. Rev. C* **78**, 035204 (2008) [arXiv:0802.3816 [nucl-th]].
- [41] J. He and B. Saghai, Combined study of $\gamma p \rightarrow \eta p$ and $\pi^- p \rightarrow \eta n$ in a chiral constituent quark approach, *Phys. Rev. C* **80**, 015207 (2009) [arXiv:0812.1617 [nucl-th]].
- [42] J. He and B. Saghai, η production off the proton in a Regge-plus-chiral quark approach, *Phys. Rev. C* **82**, 035206 (2010) [arXiv:1005.2797 [nucl-th]].
- [43] X. H. Zhong and Q. Zhao, η photoproduction on the quasi-free nucleons in the chiral quark model, *Phys. Rev. C* **84**, 045207 (2011) [arXiv:1106.2892 [nucl-th]].
- [44] X. H. Zhong and Q. Zhao, η' photoproduction on the nucleons in the quark model, *Phys. Rev. C* **84**, 065204 (2011) [arXiv:1110.5466 [nucl-th]].
- [45] L. Y. Xiao, X. Cao and X. H. Zhong, Neutral pion photoproduction on the nucleon in a chiral quark model, *Phys. Rev. C* **92**, no. 3, 035202 (2015) [arXiv:1505.06396 [nucl-th]].
- [46] T. Barnes, S. Godfrey and E. S. Swanson, Higher charmonia, *Phys. Rev. D* **72**, 054026 (2005) [hep-ph/0505002].
- [47] D. Flamm and F. Schöber, Introduction to the quark model of elementary particle, Volume 1: Quantum numbers, gauge theory and hadron spectroscopy, Gordon and Breach science publishers (1982).
- [48] Chong-Hai Cai and Lei Li, Radial equation of bound state and binding energies of Ξ^- hypernuclei, *High Energy Physics and Nuclear Physics* **27**, 1005 (2003).
- [49] A. Abdesselam *et al.*, Study of $\chi_{bJ}(1P)$ Properties in the Radiative $\Upsilon(2S)$ Decays, arXiv:1606.01276 [hep-ex].
- [50] P. del Amo Sanchez *et al.* [BaBar Collaboration], Observation of the $\Upsilon(1^3D_J)$ Bottomonium State through Decays to $\pi^+\pi^-\Upsilon(1S)$, *Phys. Rev. D* **82**, 111102 (2010) [arXiv:1004.0175 [hep-ex]].
- [51] C. Cawthfield *et al.* [CLEO Collaboration], Experimental study of $\chi_b(2P) \rightarrow \pi\pi\chi_b(1P)$, *Phys. Rev. D* **73**, 012003 (2006) [hep-ex/0511019].
- [52] R. Mizuk *et al.* [Belle Collaboration], Evidence for the $\eta_b(2S)$ and observation of $h_b(1P) \rightarrow \eta_b(1S)\gamma$ and $h_b(2P) \rightarrow \eta_b(1S)\gamma$, *Phys. Rev. Lett.* **109**, 232002 (2012) [arXiv:1205.6351 [hep-ex]].
- [53] A. M. Badalian and B. L. G. Bakker, Dominant spin-orbit effects in radiative decays $\Upsilon(3S) \rightarrow \gamma\chi_{bJ}(1P)$, *Phys. Rev. D* **86**, 074001 (2012) [arXiv:1203.0936 [hep-ph]].
- [54] G. Aad *et al.* [ATLAS Collaboration], Observation of a new χ_b state in radiative transitions to $\Upsilon(1S)$ and $\Upsilon(2S)$ at ATLAS, *Phys. Rev. Lett.* **108**, 152001 (2012) [arXiv:1112.5154 [hep-ex]].
- [55] V. M. Abazov *et al.* [D0 Collaboration], Observation of a narrow mass state decaying into $\Upsilon(1S)\gamma$ in $p\bar{p}$ collisions at $\sqrt{s} = 1.96$ TeV, *Phys. Rev. D* **86**, 031103 (2012) [arXiv:1203.6034 [hep-ex]].
- [56] R. Aaij *et al.* [LHCb Collaboration], Measurement of the $\chi_b(3P)$ mass and of the relative rate of $\chi_{b1}(1P)$ and $\chi_{b2}(1P)$ production, *JHEP* **1410**, 88 (2014) [arXiv:1409.1408 [hep-ex]].
- [57] R. Aaij *et al.* [LHCb Collaboration], Study of χ_b meson production in pp collisions at $\sqrt{s} = 7$ and 8 TeV and observation of the decay $\chi_b(3P) \rightarrow \Upsilon(3S)\gamma$, *Eur. Phys. J. C* **74**, no. 10, 3092 (2014) [arXiv:1407.7734 [hep-ex]].

TABLE IV: Partial widths of the radiative transitions for the nS - and nP -wave ($n = 2, 3$) bottomonium states. For comparison, the measured values (MeV) from the PDG [7], the predictions from the relativistic quark model [13], relativized quark model [9], nonrelativistic constituent quark model [10], and the previous screened potential model [8] are listed in the table as well.

Initial state	Final state	E_γ (MeV)				Γ_{EI} (keV)					Γ_{EM} (keV)	
		Ref.[13]	SNR _{0,1} [8]	GI [9]	ours	Ref.[13]	SNR ₀ [8]	SNR ₁ [8]	GI [9]	Ref. [10]	Ours	Exp. [7]
$\Upsilon(2^3S_1)$	$\chi_{b2}(1^3P_2)$	109	110	110	110	2.46	2.62	2.46	1.88	2.08	2.62	2.29 ± 0.20
	$\chi_{b1}(1^3P_1)$	130	130	129	129	2.45	2.54	2.08	1.63	1.84	2.17	2.21 ± 0.19
	$\chi_{b0}(1^3P_0)$	162	163	163	163	1.62	1.67	1.11	0.91	1.09	1.09	1.22 ± 0.11
$\eta_b(2^1S_0)$	$h_b(1^1P_1)$	98	83	99	99	3.09	6.10	5.57	2.48	2.85	3.41	
$\Upsilon(3^3S_1)$	$\chi_{b2}(2^3P_2)$	86	86	86	86	2.67	3.23	3.04	2.30	2.56	3.16	2.66 ± 0.27
	$\chi_{b1}(2^3P_1)$	100	99	100	100	2.41	2.96	2.44	1.91	2.13	2.61	2.56 ± 0.26
	$\chi_{b0}(2^3P_0)$	123	122	121	121	1.49	1.83	1.23	1.03	1.21	1.21	1.20 ± 0.12
	$\chi_{b2}(1^3P_2)$	433	434	434	434	0.097	0.25	1.26	0.45	0.083	0.14	0.20 ± 0.03
	$\chi_{b1}(1^3P_1)$	453	452	452	452	0.067	0.17	0.14	0.05	0.16	0.0005	0.018 ± 0.010
	$\chi_{b0}(1^3P_0)$	484	484	484	484	0.027	0.07	0.05	0.01	0.15	0.097	0.055 ± 0.010
$\eta_b(3^1S_0)$	$h_b(2^1P_1)$	73	74	77	78	2.78	11.0	10.1	2.96	2.60	4.25	
	$h_b(1^1P_1)$	427	418	429	429	0.348	1.24	5.68	1.30	0.0084	0.67	
$\chi_{b2}(2^3P_2)$	$\Upsilon(1^3D_3)$	108	113	97	101	2.35	3.33	3.13	1.5	2.06	2.51	
	$\Upsilon(1^3D_2)$	111	117	104	104	0.449	0.66	0.58	0.3	0.35	0.42	
	$\Upsilon(1^3D_1)$	117	123	113	111	0.035	0.05	0.04	0.03	0.021	0.026	
	$\Upsilon(2^3S_1)$	243	243	243	243	16.7	18.8	14.2	14.3	17.50	15.7	15.1 ± 5.6
	$\Upsilon(1^3S_1)$	776	777	777	777	8.02	13.0	12.5	8.4	11.38	13.6	9.8 ± 2.3
$\chi_{b1}(2^3P_1)$	$\Upsilon(1^3D_2)$	98	104	91	91	1.56	2.31	2.26	1.2	1.26	0.50	
	$\Upsilon(1^3D_1)$	104	110	100	98	0.615	0.92	0.84	0.5	0.41	0.56	
	$\Upsilon(2^3S_1)$	230	230	229	229	14.7	15.9	13.8	13.3	15.89	15.7	19.4 ± 5.0
$\chi_{b0}(2^3P_0)$	$\Upsilon(1^3S_1)$	764	764	764	764	7.49	12.4	8.56	5.5	9.13	11.7	8.9 ± 2.2
	$\Upsilon(1^3D_1)$	81	87	78	78	1.17	1.83	1.85	1.0	0.74	1.77	
	$\Upsilon(2^3S_1)$	207	207	208	208	11.0	11.7	11.6	10.9	12.80	14.4	
$h_b(2^1P_1)$	$\Upsilon(1^3S_1)$	743	743	744	744	6.79	11.4	4.50	2.5	5.44	5.54	
	$\eta_{b2}(1^1D_2)$	102	104	95	95	2.43	7.74	7.42	1.7	5.36	2.24	
	$\eta'_b(2^1S_0)$	262	266	258	258	21.4	24.7	15.3	14.1	17.60	16.6	
	$\eta_b(1^1S_0)$	820	831	826	826	9.36	15.9	18.0	13.0	14.90	17.5	
$\chi_{b2}(3^3P_2)$	$\Upsilon(2^3D_3)$		97	73	93		5.05	4.69	1.5	4.16	4.60	
	$\Upsilon(2^3D_2)$		101	79	97		1.02	0.89	0.32	0.79	0.78	
	$\Upsilon(2^3D_1)$		107	87	103		0.08	0.07	0.027	0.18	0.049	
	$\Upsilon(1^3D_3)$		377	350	365		0	0.05	0.046	0.21	0.12	
	$\Upsilon(1^3D_2)$				358					0.044	0.068	
	$\Upsilon(1^3D_1)$				366					0.0034	0.047	
	$\Upsilon(3^3S_1)$		183	172	173		15.6	11.1	9.3	10.38	10.8	
	$\Upsilon(2^3S_1)$		504	493	494		6.00	6.89	4.5	5.62	6.72	
	$\Upsilon(1^3S_1)$		1024	1014	1014		7.09	6.76	2.8	5.65	8.17	
	$\Upsilon(2^3D_2)$		86	67	84		3.10	2.98	1.1	3.34	0.94	
$\chi_{b1}(3^3P_1)$	$\Upsilon(2^3D_1)$		92	75	90		1.26	1.13	0.47	1.26	1.07	
	$\Upsilon(1^3D_2)$		366	346	346		0	0.09	0.08	0.11	0.015	
	$\Upsilon(1^3D_1)$		372	355	355		0	0.00	0.007	0.048	0.010	
	$\Upsilon(3^3S_1)$		167	160	160		12.0	9.97	8.4	9.62	10.3	
	$\Upsilon(2^3S_1)$		489	481	481		5.48	5.39	3.1	4.58	5.63	
	$\Upsilon(1^3S_1)$		1010	1003	1003		6.80	3.39	1.3	4.17	6.41	
	$\Upsilon(2^3D_1)$			59	68				1.0	3.50	2.20	
	$\Upsilon(1^3D_1)$		351	339	341		0	0.17	0.20	0.036	0.15	
$\chi_{b0}(3^3P_0)$	$\Upsilon(3^3S_1)$		146	144	135		7.88	7.67	6.9	8.50	7.95	
	$\Upsilon(2^3S_1)$		468	466	458		4.80	3.67	1.7	2.99	2.55	
	$\Upsilon(1^3S_1)$		990	988	980		6.41	0.86	0.3	1.99	1.87	
	$\eta_{b2}(2^1D_2)$			69	88				1.6	4.72	4.21	
	$\eta_{b2}(1^1D_2)$		370	348	360		0	0.24	0.081	0.35	0.17	
	$\eta_b(3^1S_0)$		196	180	194		19.2	11.6	8.9	12.27	14.1	
$h_b(3^1P_1)$	$\eta_b(2^1S_0)$		528	507	508		6.89	10.3	8.2	6.86	7.63	
	$\eta_b(1^1S_0)$		1078	1061	1062		8.27	9.46	3.6	7.96	10.7	

TABLE V: Partial widths of the radiative transitions for the $1P$ -, $1D$ - and $2D$ -wave bottomonium states. For comparison, the predictions from the relativistic quark model [13], relativized quark model [9], nonrelativistic constituent quark model [10], and previous screened potential model [8] are listed in the table as well.

Initial meson state	Final meson state	E_γ (MeV)				Γ_{E1} (keV)					Γ_{EM} (keV)
		Ref.[13]	SNR _{0,1} [8]	GI [9]	ours	Ref.[13]	SNR ₀ [8]	SNR ₁ [8]	GI [9]	Ref. [10]	Ours
$\chi_{b2}(1^3P_2)$	$\Upsilon(1^3S_1)$	442	442	442	442	40.2	38.2	32.6	32.8	39.15	31.8
$\chi_{b1}(1^3P_1)$		422	423	424	424	36.6	33.6	30.0	29.5	35.66	31.9
$\chi_{b0}(1^3P_0)$		391	391	391	391	29.9	26.6	24.3	23.8	28.07	27.5
$h_b(1^1P_1)$	$\eta_b(1^1S_0)$	480	501	488	488	52.6	55.8	36.3	35.7	43.66	35.8
$\Upsilon(1^3D_3)$	$\chi_{b2}(1^3P_2)$	244	240	257	253	24.6	26.4	24.5	24.3	24.74	32.1
	$\chi_{b1}(1^3P_1)$				271					0	1.1×10^{-2}
	$\chi_{b0}(1^3P_0)$				304					0	9.2×10^{-5}
$\Upsilon(1^3D_2)$	$\chi_{b2}(1^3P_2)$	241	236	249	249	6.35	6.29	5.87	5.6	6.23	7.23
	$\chi_{b1}(1^3P_1)$	262	255	267	267	23.3	23.8	19.8	19.2	21.95	21.8
	$\chi_{b0}(1^3P_0)$				300					0	0.83×10^{-2}
$\Upsilon(1^3D_1)$	$\chi_{b2}(1^3P_2)$	235	230	240	242	0.69	0.65	0.61	0.56	0.65	1.02
	$\chi_{b1}(1^3P_1)$	256	249	259	261	12.7	12.3	10.3	9.7	12.29	13.3
	$\chi_{b0}(1^3P_0)$	280	282	292	294	23.4	23.6	16.7	16.5	20.98	19.8
$\eta_{b2}(1^1D_2)$	$h_b(1^1P_1)$	254	246	263	262	28.4	42.3	36.5	24.9	17.23	30.3
$\Upsilon(2^3D_3)$	$\chi_{b2}(1^3P_2)$		517	529	511		4.01	3.73	2.6	3.80	5.22
	$\chi_{b1}(1^3P_1)$				535					0	0.16
	$\chi_{b0}(1^3P_0)$				567					0	0.08
	$\chi_{b2}(2^3P_2)$		172	184	166		18.0	15.9	16.4	10.70	17.0
	$\chi_{b1}(2^3P_1)$				185					0	0.34×10^{-2}
	$\chi_{b0}(2^3P_0)$				207					0	0.66×10^{-3}
$\Upsilon(2^3D_2)$	$\chi_{b2}(1^3P_2)$		513	523	507		0.98	0.68	0.4	0.80	1.11
	$\chi_{b1}(1^3P_1)$		531	541	525		3.26	4.46	2.6	3.43	4.00
	$\chi_{b0}(1^3P_0)$				555					0	0.89×10^{-2}
	$\chi_{b2}(2^3P_2)$		168	178	162		4.17	3.82	3.8	2.55	3.75
	$\chi_{b1}(2^3P_1)$		181	192	175		15.7	12.1	12.7	9.10	11.4
	$\chi_{b0}(2^3P_0)$				197					0	1.7×10^{-3}
$\Upsilon(2^3D_1)$	$\chi_{b2}(1^3P_2)$		507	516	500		0.11	0.05	0.9	0.061	0.44
	$\chi_{b1}(1^3P_1)$		525	534	518		1.76	1.87	2.9	1.58	2.17
	$\chi_{b0}(1^3P_0)$		557	566	551		2.79	6.20	1.6	3.52	5.56
	$\chi_{b2}(2^3P_2)$		162	171	155		0.42	0.39	0.4	0.24	0.47
	$\chi_{b1}(2^3P_1)$		175	184	167		7.87	6.35	6.5	4.84	6.74
	$\chi_{b0}(2^3P_0)$		198	206	190		15.1	9.49	10.6	8.35	9.58
$\eta_{b2}(2^1D_2)$	$h_b(1^1P_1)$		522	536	519		6.19	7.30	3.0	4.15	5.66
	$h_b(2^1P_1)$		181	188	171		31.3	25.4	16.5	11.66	15.6